Effect of bias voltage on the tribological and sealing properties of rubber seals modified by DLC films

Liu, JiaQi; Wu, Zhiyu; Cao, Huatang; Wen, Feng; Pei, Yutao T.

Published in:
Surface and Coatings Technology

DOI:
10.1016/j.surfcoat.2018.12.100

Surface & Coatings Technology 360 (2019) 391–399

Contents lists available at ScienceDirect

Surface & Coatings Technology

journal homepage: www.elsevier.com/locate/surfcoat

Effect of bias voltage on the tribological and sealing properties of rubber seals modified by DLC films

J.Q. Liu[a], Z.Y. Wu[a], H.T. Cao[b], F. Wen[a,*], Y.T. Pei[b]

[a] Key Lab. of Advanced Material of Tropical Island Resources of Educational Ministry, School of Material and Engineering, Hainan University, Haikou 570228, P.R. China
[b] Department of Advanced Production Engineering, Engineering and Technology Institute Groningen, University of Groningen, Nijenborgh 4, 9747, AG, the Netherlands

ARTICLE INFO

Keywords:
Diamond-like carbon film
Nitrile butadiene rubber
Tribology
Sealing property
Contact mechanics

ABSTRACT

Diamond-like carbon (DLC) films were deposited on nitrile butadiene rubber (NBR) by the DC magnetron sputtering under different bias voltages. Raman spectra revealed that the variation of bias voltage could tune the carbon bond structure in DLC films. Both the hardness and Young's modulus increased with the increasing bias voltage. Tribological tests revealed that the DLC-coated NBR prepared at the bias voltage of −200 V exhibited low wear rate due to its high hardness. The sealing property was studied by evaluating the leakage rate of volatile liquid in a simple apparatus. All DLC films resulted in less leakage rate as compared to the raw rubber under large stress. The lowest leakage rate occurred in the DLC-coated NBR prepared with a bias voltage of −200 V, which was associated with the theoretical calculations (Persson's theory). It was attributed to the synergetic effects of the variations of the Young's modulus and root-mean-square (Rms) roughness. The low Young's modulus and Rms, controlled by regulating bias voltage, could enhance actual contact area and reduce the leakage rate.

1. Introduction

Rubber seals are ubiquitous machine parts widely used in industry for purposes of leakage prevention, pressure maintenance, dirt exclusion, and separation of various media from each other. However, the design of dynamic rubber seals involves many challenges such as minimizing the friction and wear and reducing the leakage rate, thereby reducing energy consumption and environmental pollution, and extending the service life time of seals [1]. Diamond-like carbon (DLC) film is an ideal solution as protective coatings in many applications due to its combination of relatively high hardness [2], low coefficient of friction [3] and low wear rate [4].

DLC films have been reported [5] to be applied in modification of polymer materials for a long period of time. Some reports [6–8] showed that the DLC films deposited on rubber presented an excellent anti-friction effect with low coefficient of friction and low wear rate. In addition, the sealing property is also crucial in the field of rubber seals. Persson [9] substantially studied the rubber contact theory and leak rate analysis, and found how leakage rate depends on the root-mean-square roughness amplitude and the fractal dimension, and on the stress with which the rubber is squeezed against the countersurface. However, in the field of coatings, it is still unclear whether the surface coating will affect the sealing performance of rubber.

Furthermore, the mechanical properties of DLC films, for instance, the hardness and elastic modulus mainly depend on the sp^3 bond fraction, which are strongly dependent upon the kinetic energy of incident particles arriving at the substrate during deposition [10]. The mechanical property of DLC films deposited on rubber is very unique due to the challenging mismatching between substrate and film. Meanwhile, the role of bias voltage on the sealing property is not yet clearly understood.

This research aims to study the effect of bias voltage on tribological performance and sealing property of DLC-coated rubber combined with contact mechanics of rough surface, so as to design workable high-performance rubber seals.

2. Experimental section

2.1. Deposition of DLC films

The nitrile butadiene rubber (NBR) were initially cleaned by two steps using a detergent solution and boiling water, respectively, in order to remove the dirt and the wax on the rubber and also improve the film adhesions with the substrate [11]. Both the silicon (100) wafers and

* Corresponding author at: Key Lab. of Advanced Material of Tropical Island Resources of Educational Ministry, School of Material and Engineering, Hainan University, Haikou 570228, P.R. China.
E-mail address: fwen323@163.com (F. Wen).

https://doi.org/10.1016/j.surfcoat.2018.12.100
Received 29 August 2018; Received in revised form 21 December 2018; Accepted 25 December 2018
Available online 28 December 2018

NBR were dried in vacuum oven after being ultrasonically cleaned 10 min for 3 times. Note that part of silicon wafer was covered with a shield silicon wafer for later measurement of the film thickness.

Prior to deposition, the substrates were pre-sputtered for cleaning for 5 min at 3 Pa using argon ions, guided by an anode with a bias voltage of −600 V, at a frequency of 40 kHz and a duty ratio of 75%. Then DLC films were deposited simultaneously on NBR and silicon wafers using DC magnetron sputtering without substrate heating applied. A graphite (> 99.9%) target was sputtered at a power of 100 W in atmosphere of argon gas, and the pressure in the chamber was kept at 1.4 Pa. A batch of DLC films were produced with four different pulse bias voltages applied on substrates of 0, −50, −100 and −200 V, respectively at a frequency of 40 kHz and a duty ratio of 75%. The deposition time of each sample was 25 min. Besides, the cleaned pristine NBR substrates were also prepared for comparisons in follow-up experiments.

2.2. Materials characterization

The structure and chemical bonding configurations of DLC films were analyzed using Raman spectroscopy (inVia Reflex, Renishaw) with incident lights at a wavelength of 514.5 nm. The nanoindentation tests were implemented with a Berkovich diamond tip (CETR-UMT, Bruker). A load of 1 mN was applied linearly up to the maximum load in 15 s with a creep procedure of 10 s followed by unloading in 15 s. The thermal drift was set to remain invariable load for 45 s when unloading to 0.1 mN. For each sample five indentations were performed on five different areas. And each two indentations were spaced by 20 μm in order to avoid any effects of residual stress from the neighboring indentations.

The tribological properties of the samples were investigated using a ball-on-disk tribometer (CETR-UMT, Bruker) under dry condition at room temperature. Each sample was tested against a tungsten carbide ball of Φ1.6 mm in a circular path of Φ9 mm at a speed of 100 rpm under a normal load of 0.3 N. Each trial lasted for 2 h. The surface profiles of the wear tracks were determined by a Dektak-XT surface profiler (Bruker) with a stylus force of 3 mg over a scanning range of 12 mm. The thickness of DLC films on silicon wafers was also determined by the Dektak-XT surface profiler (Bruker) with a stylus force of 3 mg over a scanning range of 2 mm. A digital camera (ZNZ500-A4CS, Senmike) and an optical microscopy were used to observe wear tracks.

The surface topography of the as-deposited films was revealed by adopting atomic force microscopy (AFM, Nanosurf AG) via a tapping mode with a silicon probe (Tap 190Al-G). Areas of $5 \times 5\,\mu m^2$ for each sample were employed for the general observation. A scanning electron microscope (SEM, Hitachi S-4800) was also used to observe the imprint after sealing tests.

2.3. Set-up for sealing property

Fig. 1 showed the home-made set-up for evaluating the sealing property of rubber. A glass bottle (the inner and outer diameters of bottleneck were 11.8 mm and 15.4 mm, respectively) with a rubber bulk attached to one end was covered against a mass. In this case, we chose a stainless-steel plate (12 × 12 × 4 mm in dimension) with a total mass of 460 g, in order to balance the stress better with large mass area. The glass bottle with a total volume of 13.0 mL was filled with a volatile liquid (e.g. 5.000 g of ethanol here). The leakage of the fluid at the rubber counter surface was detected by measuring the difference in the mass of the fluid in the glass bottle by an electronic balance (BSM-320.3, accuracy = 0.001 g). Here the pressure difference between the inside and outside of the glass bottle was given by vapor pressure (5.8 kPa at 20 °C for ethanol [12]) of the volatile liquid, which triggered the leakage. It was important to note that the ultimate weight of leakage was determined as a result of the decreased weight in bottle minus the increased weight in rubber, taking the adsorption on rubber surface into consideration.

3. Results and discussion

3.1. Raman spectroscopy

The Raman spectra of DLC films deposited with different bias voltages are shown in Fig. 2. In general, a typical composite band for DLC film existed around 1500 cm^{-1} in Raman spectrum. In the irreducible representation of the Brillouin zone dot center optical model, double degenerate mode E_{2g} was activated by Raman, and one of the main Raman shifts was situated in 1582 cm^{-1}, generally known as G mode. For disordered carbon structure, there was another first-order Raman shift which was a result of hexagon Brillouin zone boundary exactly. The peak position located at 1360 cm^{-1} is often referred as D mode, which was caused by the disorder structure [13]. Note there seemed to be a peak around 1415 cm^{-1} in Raman spectra, which was attributed to the aromatic substitution groups in NBR. Consequently, the Raman spectra were deconvoluted into three Gaussian peaks, including the peaks near 1330 cm^{-1} and 1580 cm^{-1}, corresponding to D peak and G peak, respectively.

The areas of D peak and G peak were calculated to represent their intensities, marked as I_D and I_G, respectively. The sp^2/sp^3 ratio can be inferred through the ratios of the values for I_D/I_G according to Ferrari's work [14]. The effect of bias voltage on the sp^2/sp^3 ratio was shown in Fig. 3. The less the I_D/I_G value, the smaller the sp^2/sp^3 ratio. When the bias voltage changed from 0 to −100 V, the sp^2/sp^3 ratio decreased. It can be explained by the sub-surface implantation model [15]. When the applied bias voltage increased from 0 to −100 V, the incoming ions had sufficient energy to penetrate the outer layers of growing films and gave rise to a local densification where the bonding will convert to sp^3 C—C hybridized bonding. However, for the films deposited under further negative bias voltage of −200 V, the excess ion energy promoted atomic relaxation around the implanted atom and a reversion of diamond-like sp^3 bonding to graphite-like sp^2 bonding [16]. Therefore, the bias voltage can control the compositions and chemical state of prepared DLC films.

3.2. Nanoindentation

Fig. 4 showed the typical indentation load-depth curves for both NBR and DLC-coated NBR with different bias voltages. The Oliver and Pharr method [17] is based on purely elastic contact procedure. However, in terms of NBR, the contact between an indenter tip and a semi-infinite body is viscoelastic (exhibiting simultaneously viscous flow and elasticity behavior). One study [18] showed that creep occurring during the nanoindentation unloading can lead to an overestimation of Young's modulus. One of the commonly used methods to take into account the viscoelastic properties of polymeric materials during nanoindentation is to hold the indenter at the maximum load for a period of time [19,20]. This, however, will lead to creep effects during indentation. Under the circumstances the measured elastic modulus and hardness are dependent of holding time, maximum load, and loading/unloading rates [21].

According to Qian et al. [22], the smaller error in modulus and hardness calculated by Oliver and Pharr method is strongly associated with larger nanoindentation depth (> 800 nm) in polymer, because of the incomplete recovery after unloading to zero. It can be seen that the maximum depth of indentation on every sample was obviously different. All DLC-coated NBR exhibited larger maximum depth as compared with bare NBR. The maximum depth increased with the decreasing bias voltage. It can be also found that residual depth of every sample was roughly the same, even though the maximum depths were very different. Therefore, the elastic recovery ratio of samples exhibited similar trends as the maximum depth did. The recovery ratio R can be calculated as [23]:

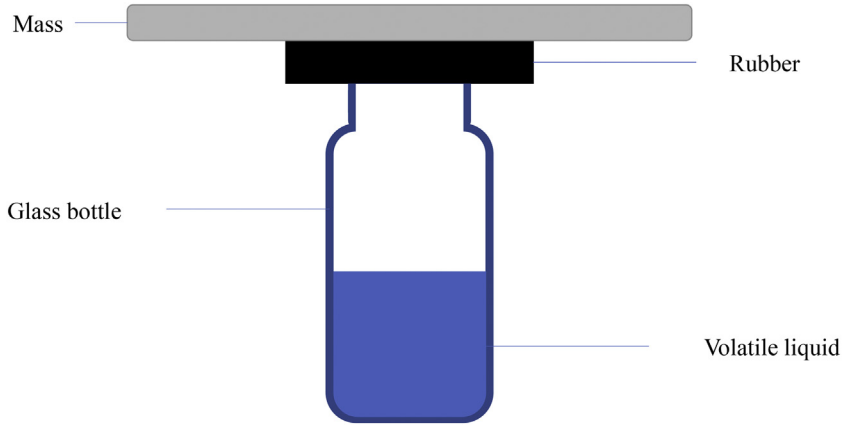

Fig. 1. Experimental set-up for evaluating the sealing property of rubber. The contact stress between rubber and bottle arises from the gravity of both mass and rubber.

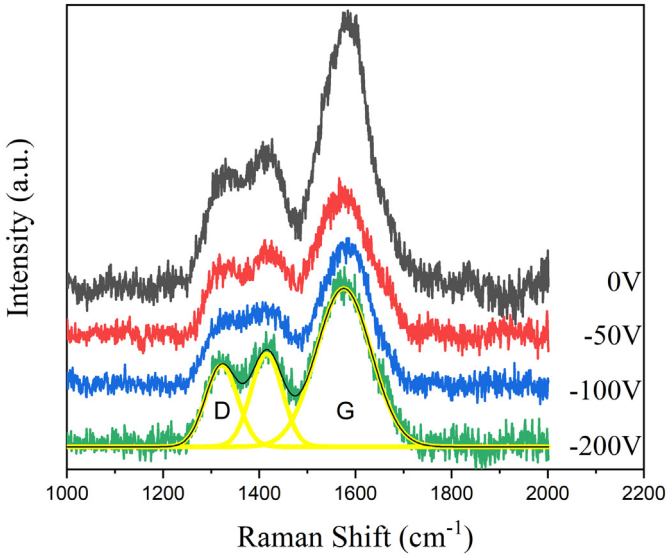

Fig. 2. Raman spectra (514.5 nm) of DLC films on NBR with different bias voltages. The spectrum can be fitted with Gaussian line shapes to three peaks, indicated by the yellow line. (For interpretation of the references to color in this figure legend, the reader is referred to the web version of this article.)

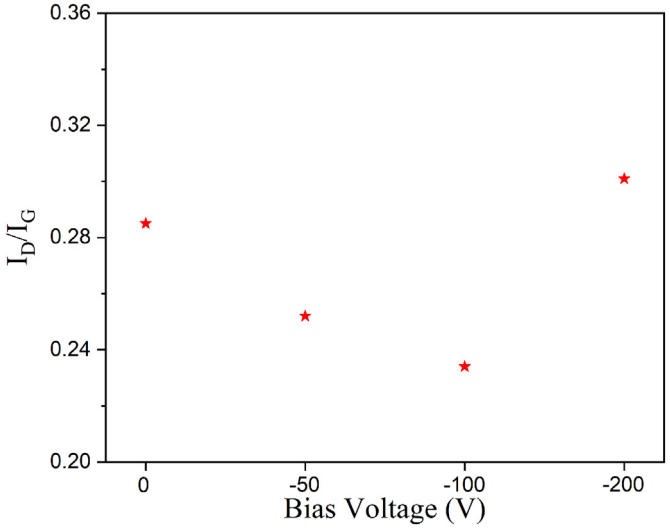

Fig. 3. I_D/I_G ratio of DLC films prepared at different bias voltages.

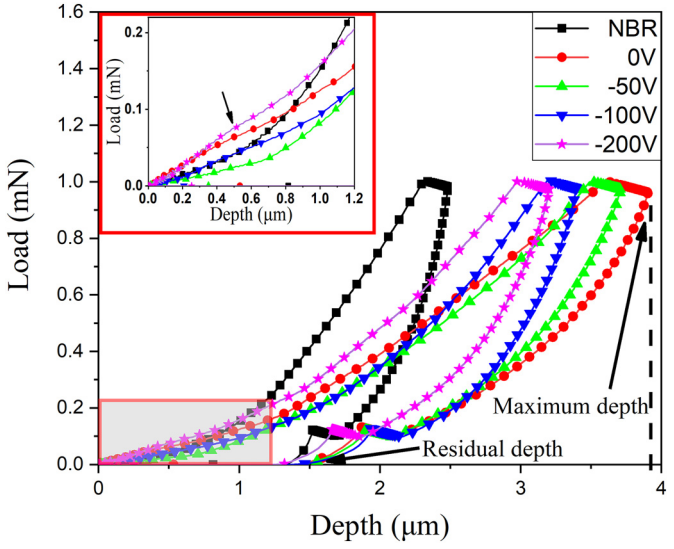

Fig. 4. Load-depth curves for NBR and DLC-coated NBR deposited at different bias voltages. The inset is a close-view of the area marked with a red rectangle. (For interpretation of the references to color in this figure legend, the reader is referred to the web version of this article.)

$$R = (h_{max} - h_{res})/h_{max} \times 100\%, \quad (1)$$

where h_{max} and h_{res} are the maximum depth at the maximum load and the residual depth after unloading, respectively. In addition, it can be stated that there was always a reduction in the slope of curves excluding the curve of NBR (see the inset in Fig. 4), which probably arose from the influence of DLC film.

Hardness and Young's modulus were calculated by Oliver and Pharr method on the basis of load-depth curves. It was important to note that the result of modulus was a reduced modulus. The reduced modulus E^* is related to Young's modulus E of the test specimen through the following relationship from contact mechanics [24]:

$$1/E^* = (1 - \nu_{tip}^2)/E_{tip} + (1 - \nu^2)/E. \quad (2)$$

Here, the subscript tip indicates a property of the indenter material and ν is Poisson's ratio. In this work, the reduced modulus data were transformed into Young's modulus following Eq. (2), taking a value of $\nu = 0.5$ for NBR as previously reported in Ref. [25]. Since maximum depth exceeded greatly the film thickness, the calculated Young's modulus and hardness values were considered to represent a mixture of film and substrate [26].

The Fig. 5 plots the variations of hardness and Young's modulus of

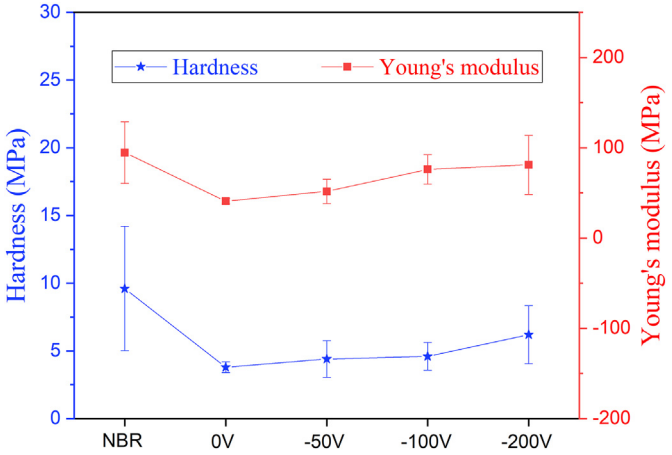

Fig. 5. Variation of the hardness and Young's modulus of NBR and DLC-coated NBR deposited under different bias voltages.

NBR and DLC-coated NBR prepared with different bias voltages. It was observed that there was a drop in both hardness and Young's modulus when NBR was coated with DLC. Generally, the hardness is strongly related to the maximum area subjected to the maximum depth. The dip in the measured Young's modulus may be ascribed to the breakthrough of the film and a sudden advance of tip into the substrate [27]. Meanwhile, the Young's modulus closely tracked the hardness variations, with both hardness and Young's modulus increasing with the increasing bias voltage. This was in good agreement with the Raman results.

3.3. Tribology

The curves of on-going coefficient of friction (COF) versus number of sliding cycle are shown in Fig. 6. Obviously, all prepared DLC films resulted in decreased COF values before 4000 laps, suggesting the improved tribological performance. As the laps increased, the temperature of rubber increased such that rubber molecules became easier to move due to thermal motion and thereby reduced the hysteresis friction. Thus, all COF curves showed downward trends in the late period of sliding. In the whole tests, the wear debris of DLC can promote the formation of transfer layers to reduce friction [28,29], ultimately resulting in an ultralow COF approaching 0.05 in the DLC-coated NBR with a bias voltage of −100 V in particular.

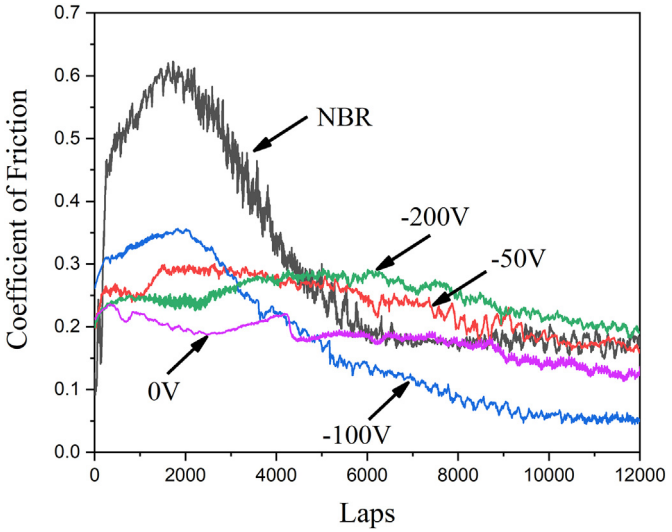

Fig. 6. Evolution of coefficient of friction as a function of laps.

The typical wear track after dry sliding under a load of 0.3 N of the DLC-coated NBR with a bias voltage of −200 V was shown in Fig. 7(b). It can be seen that severe nonuniformity occurred in the wear track, which can be explained by the high deformation and elasticity of the rubber substrate [30]. Meanwhile, the elaborate megascopic illustrations were also placed in Fig. 7, which compared the differences of two sides in the wear track. The width of narrow side was about 266 μm, while that was close to 466 μm for the other side.

In order to explore the wear conditions in detail, the wear profiles were obtained by tracing the blue lines, including the maximum and minimum of wear width. Fig. 8 showed the wear profiles of the wear tracks, which also indicated nonuniformity of the wear tracks attributed to the difference in wear depth H_1 and H_2 on both sides of the diameter. Then the wear volume of every sample was calculated by two methods:

a. Assuming the sectional area changes linearly over periphery from S_1 to S_2 on both sides. Then the volume can be obtained by integrating.
b. Assuming the wear tracks are similar to the profile of grinding ball and the sectional depth changes linearly over periphery from H_1 to H_2 on both sides. Then the volume can be obtained by integrating.

The calculated wear volumes of all samples were shown in Fig. 9. There was a minor difference between the two methods, consolidating the reliability of results. All the DLC-coated NBR exhibited less wear volume compared with the pristine NBR, revealing improved wear resistance after depositing DLC films. It was also found that the effect of bias voltage on wear resistance was significant. The wear volumes of DLC-coated NBR with bias voltage of 0 V and −200 V were obviously less than those with other bias voltages applied. It was important to note that wear volume was strongly related to the thickness of DLC films. But in this case, the thickness of each film was different under various bias voltages, although the deposition time was identical. In addition, the thickness of the thin films on the rubber substrate was hard to evaluate. Therefore, the thickness of identical DLC films on silicon wafer was measured as reference (shown in Fig. 9). The film thickness exhibited a decrease from 19.53 nm to 0 nm as the bias voltage varied from 0 to −200 V. This was due to the increased ion bombardment with a higher energy flux at a more negative voltage, resulting in a lower deposition rate [31]. Thus, the less wear volume with the bias voltage of 0 V was attributed to its large thickness [32]. Ignoring the effect of thickness, the films prepared under a more negative bias voltage would have better wear resistance due to their high hardness.

3.4. Sealing property

Firstly, the weight of mass in Fig. 1 was set as 1820 g, and the whole process lasted for 16.5 h. The weight of leakage measured was shown in Fig. 10. It can be seen that the NBR was the only one where leakage occurred. And the imprint of stress was found on all DLC-coated NBR rather than NBR. Hence, the imprint observed by SEM was also shown in Fig. 10. Many tiny cracks existed on surface after chronic stress, while the cracks on non-imprint surface were due to the flexible temperature-sensitive NBR. It should be noted that the chapped DLC hardly delaminate from the substrate. The discrete films were benefit for the deformation of film following rubber.

In order to explore the differences in various DLC-coated NBR prepared with different bias voltages, the weight of mass was reduced to 460 g and the whole process was prolonged to 24 h. The results were exhibited in Fig. 11 and there seemed to be no imprint on the surface with the smaller applied stress (0.06 MPa). It can be demonstrated that NBR still possessed highest leakage rate compared with other DLC-coated NBR. The leakage rate of all DLC-coated NBR were also distinct, among which the lowest weight of leakage occurred in the sample prepared with bias voltage of −200 V, reflecting the remarkable influence of bias voltage. The percolation channel occurred when the

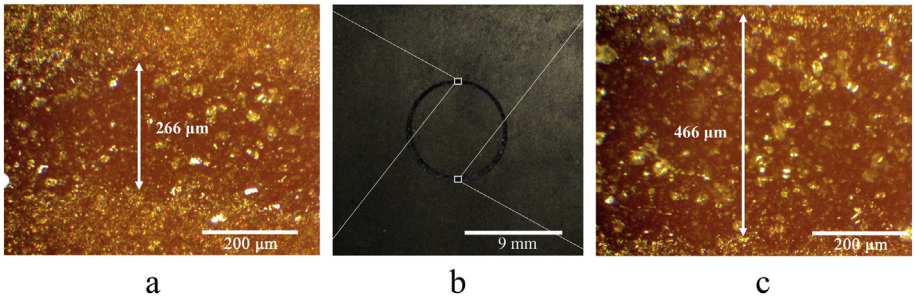

Fig. 7. Optical images of the wear tracks for the DLC-coated NBR with bias voltage of −200 V. (a) and (c) are magnified images from the narrow and broad width of wear track indicated in (b), respectively.

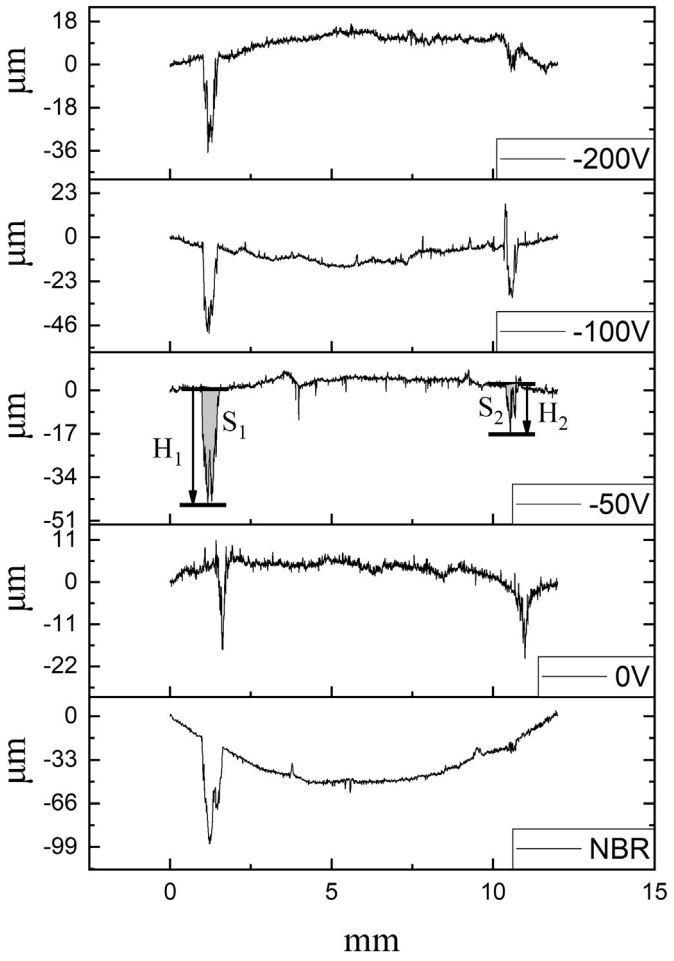

Fig. 8. Wear profiles of the wear tracks for all samples under dry sliding and a normal load of 0.3 N. H_1 and H_2 stand for the maximum and minimum wear depth, corresponding to their sectional area S_1 and S_2, respectively.

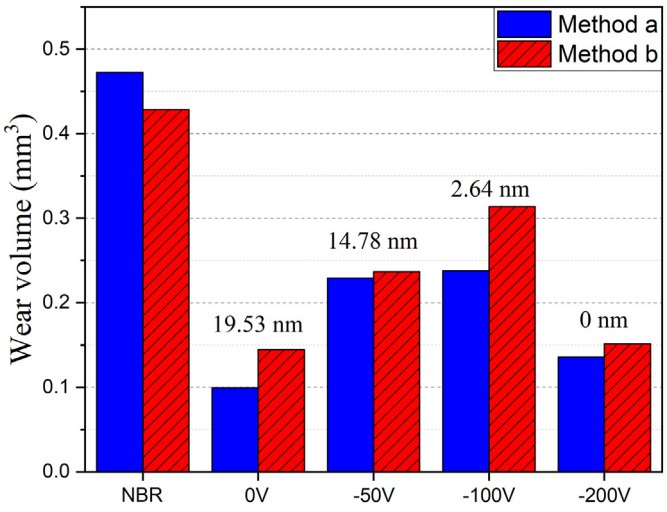

Fig. 9. Wear volume of all samples calculated by two methods on the basis of wear profile. The thickness of DLC films on silicon wafer with identical manufacturing process was given above the corresponding samples.

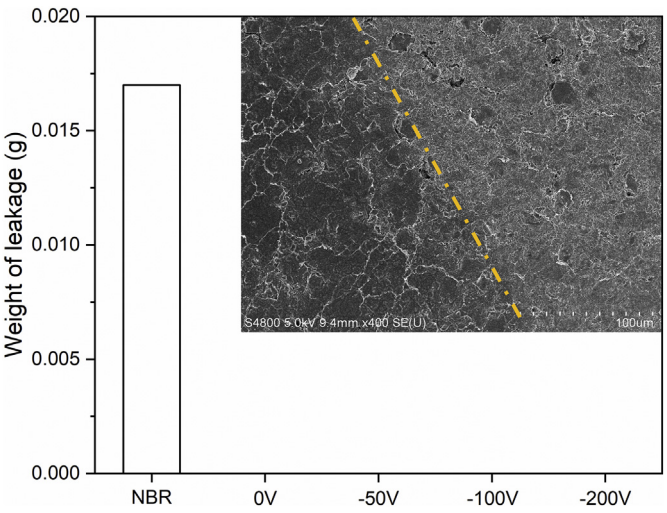

Fig. 10. The weight of leakage in glass bottle of all samples, with the mass of 1820 g, lasting for 16.5 h. The typical SEM image focused on the boundary between imprint (right) and non-imprint (left).

ratio of apparent area to nominal area decreased to a critical value, but the critical value which is statistically significant is actually indeterminate. Therefore, the error bar cover broadly. In the next moment, the factors related to leakage were investigated in detail.

According to contact mechanics of rough surface [33], the contact substrate has roughness on many different length scales and the rubber makes partial contact with the substrate on all length scales. When a contact area is studied at low magnification it appears as if complete contact occurs, but observations under high magnification may reveal that in reality only partial contact occurs.

If we study an area $A_0 = L^2$, defining the consistent magnification $\zeta = L/\lambda$, where λ is the resolution. Then the contact between two surfaces can be described as follows: at a high apparent area A(ζ), there is no consecutive channel from top to bottom in this area; as the apparent area A(ζ) decrease, a percolating path of non-contact area will eventually be observed, as seen in Fig. 12.

The relative contact area $A(\zeta)/A_0$ at the magnification ζ can be obtained using the contact mechanics formalism developed elsewhere [34]. It can be expressed as

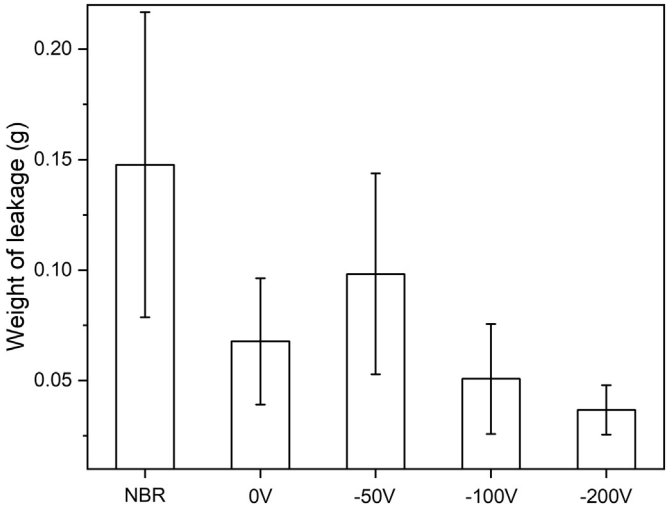

Fig. 11. The weight of leakage in glass bottle of all samples, with the mass of 460 g and the lasting time of 24 h.

$$A(\zeta)/A_0 = erf\,(P_0/2G^{1/2}), \tag{3}$$

where

$$G(\zeta) = (\pi/4)(E/(1-\nu^2))^2 \int_{q_0}^{\zeta q_0} dq\, q^3 C(q), \tag{4}$$

where the surface roughness power spectrum

$$C(q) = (1/(2\pi)^2) \int d^2x\, \langle h(\boldsymbol{x})h(\boldsymbol{0})\rangle\, exp(-i\boldsymbol{qx}), \tag{5}$$

where $\langle\cdots\rangle$ stands for ensemble average and the overstriking stands for vector. Here E and ν are the Young's modulus and the Poisson ratio of the rubber. The height profile h(**x**) of the rough surface can be measured routinely currently on all relevant length scales using optical or stylus instruments.

Many surfaces tend to be nearly self-affine fractal. A self-affine fractal surface has the property that if part of the surface is magnified, under a magnification which in general is appropriately different in the perpendicular direction to the surface as compared to the lateral directions, then the surfaces "appear the same", i.e., the statistical properties of the surface are invariant under the scale transformation [35]. For a self-affine surface, the power spectrum has the power-law behavior [33] for $q_0 < q < q_1$:

$$C(q) = C_0 q^{-2(1+H)}, \tag{6}$$

where

$$C_0 = (H/\pi)\langle h^2\rangle (q_0^{-2H} - q_1^{-2H})^{-1}, \tag{7}$$

where q_0 and q_1 are the long-distance and short-distance roll-off wave vectors, respectively. $\langle h^2\rangle$ stands for the mean of the square of the surface roughness amplitude, and Hurst exponent H is related to the fractal dimension D_f of the surface via $H = 3 - D_f$.

The surface topographies of all samples were shown in Fig. 13. As can be seen, NBR exhibited the topography of clusters attributing to formed DLC, even though the overall topography trend subjected to large roughness of NBR. It can be found that all applied DLC films resulted in low root-mean-square (Rms) surface roughness. This is likely because sputtered carbon atoms were accumulated in the hollows on the surface of NBR and filled into the hollows when DLC films were deposited on rough surfaces of NBR [36]. The result also meant that the

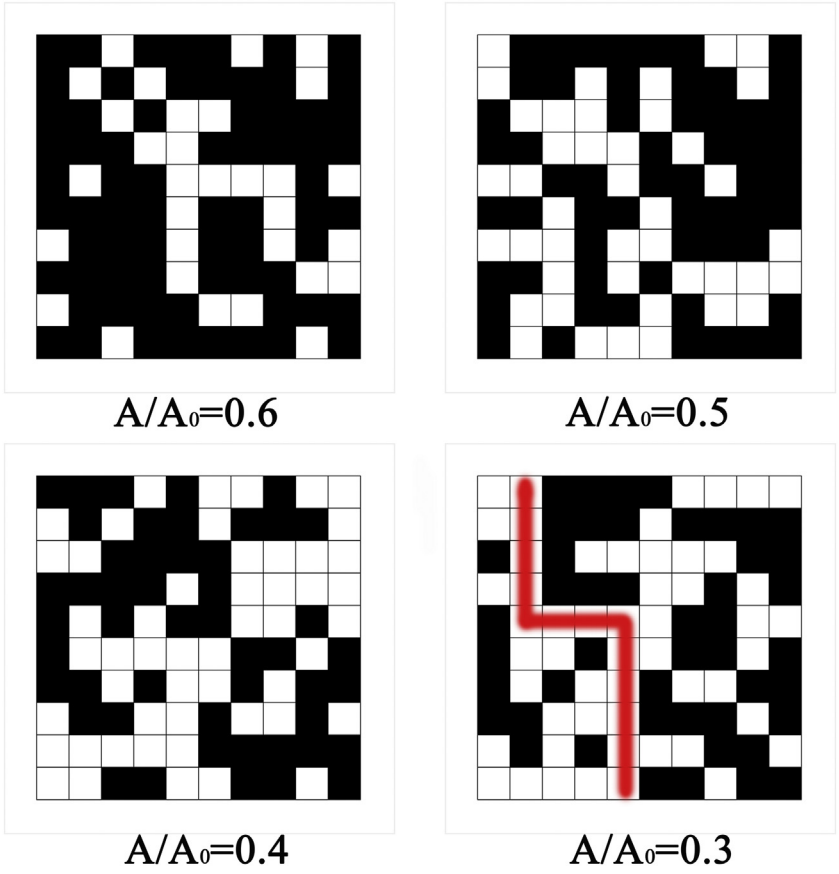

Fig. 12. Schematic of the contact region at different apparent area, where A_0 is the nominal contact area. In this case, $\zeta = 10$ and A means A(ζ). Note that at the point where the non-contact area (white area) percolates when A/A_0 decreases to 0.3.

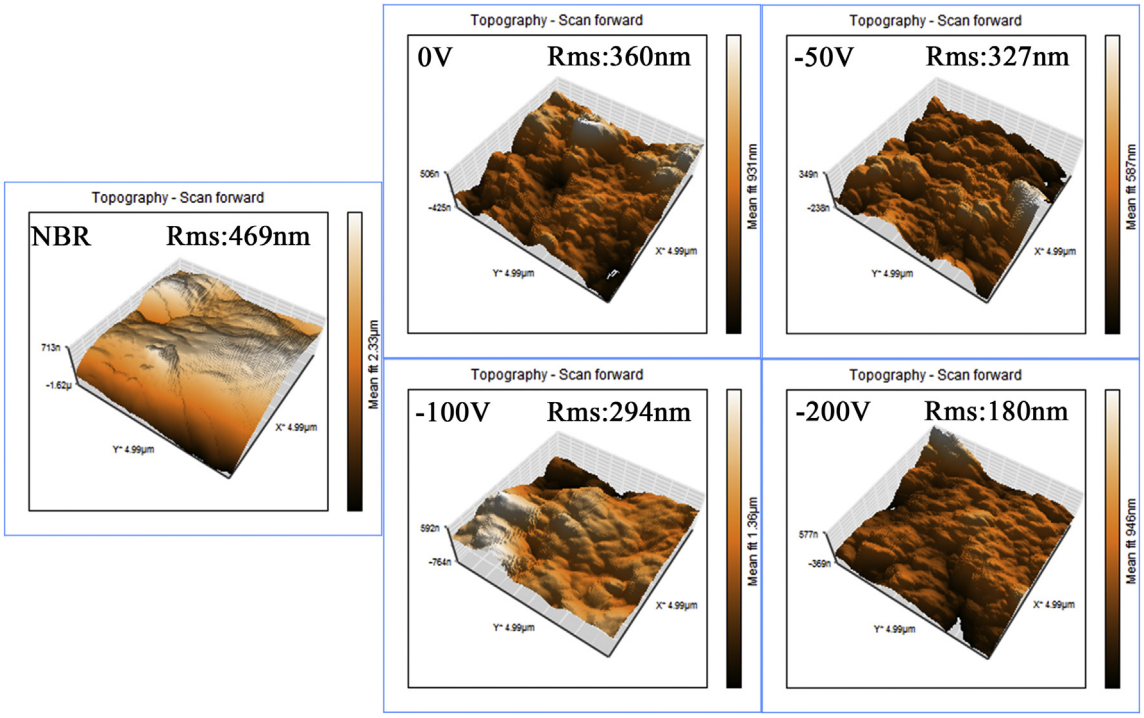

Fig. 13. AFM images (5 × 5 μm^2) of NBR and DLC-coated NBR deposited under different bias voltages, with Rms roughness provided.

DLC film deposited with an increase in bias voltage had a lower Rms roughness. It was well known that the film roughness was strongly affected by average kinetic energy of sputtered atoms [37]. When the bias voltage increased, the energy of the carbon atoms increased so that these atoms became easier to move over the substrate surface, and as a result the film tended to be compact and smooth [38].

The calculation details about surface roughness power spectrum were stated in Persson's review [35]. The typical log C - log q curve usually exhibits a slope ($q_0 < q < q_1$) after a flatline ($q_L < q < q_0$). The lateral size L of the studied surface region determines the smallest possible wave vector $q_L = 2\pi/L$ (here $L = 5$ μm), and q_0 is determined by Rms amplitude. The slope of the log C - log q relation for $q_0 < q < q_1$ determines the fractal dimension of the surface (Fig. 14). It could be stated [39] that surfaces produced by crack propagation have self-affine fractal structure with the universal fractal dimension $D_f \approx 2.2$. In our cases, it was found that the fractal dimension of all surfaces belonged to 2.1 ± 0.1, which was close to a random rough surface. Consequently, the Hurst exponent was assigned to 0.9 in all samples in order to simplify the calculation. Besides, the log C - log q relations were not perfectly straight lines, that is to say, the surfaces studied cannot be accurately described as self-affine fractals.

In this research, the variation in Rms amplitude of all samples was too small for the magnitude of log q. Therefore, the q_0 can be set by mean of average Rms amplitude: $q_0 = 2\pi/\overline{Rms}$. The ζ was set as 5000, assuring the size of smallest lattice studied can be larger than kinetic diameter of ethanol, and the stress was adopted as the mass of 460 g over nominal contact area. The $A(\zeta)/A_0$ was obtained by substituting essential parameters into Eq. (3), shown in Fig. 15. It was noted that under this ζ the actual contact area was so small compared with the nominal contact area, which implied the leakage occurred in the studied area. The smaller $A(\zeta)/A_0$ was, the larger leakage rate was. The small $A(\zeta)/A_0$ of NBR and large $A(\zeta)/A_0$ of DLC-coated NBR with bias voltage of −200 V were in good agreements with the results of experiments. Furthermore, when the stress was fixed, the crucial parameters that can influence leakage rate were primarily the Young's modulus and Rms roughness. Materials with large Young's modulus triggered small strain during contact process and thus reduced the actual contact area. Large Rms roughness could also produce this reduction. Unfortunately, the effects of bias voltage on Young's modulus and Rms roughness were diametrically opposite. But in this study, the combined effects of these two aspects gave rise to the least rate of leakage, as shown in the DLC-coated NBR prepared with a bias voltage of −200 V.

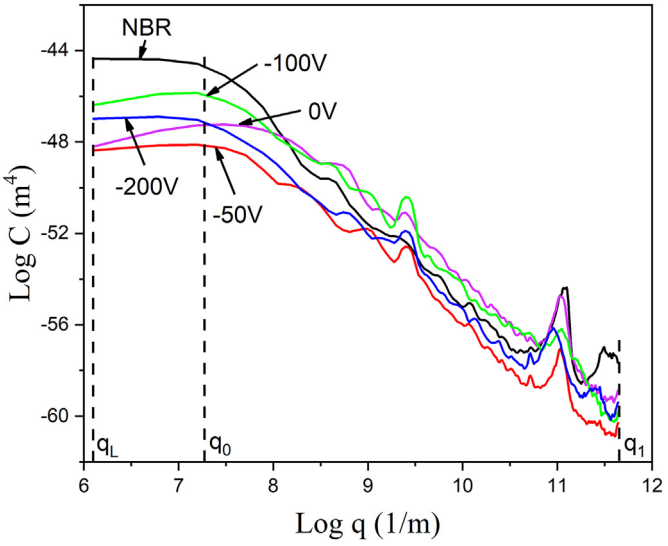

Fig. 14. The surface roughness power spectra C(q) for surfaces of all samples. The curves are based on the height profiles measured with an AFM at a spatial resolution over 5 × 5 μm square areas. The long-distance roll-off wave vector q_0 and the short distance cut-off wave vector q_1 depend on the system under consideration. The lateral size L of the studied surface region determines the smallest possible wave vector $q_L = 2\pi/L$.

4. Conclusions

In this work, diamond-like carbon (DLC) films deposited on nitrile

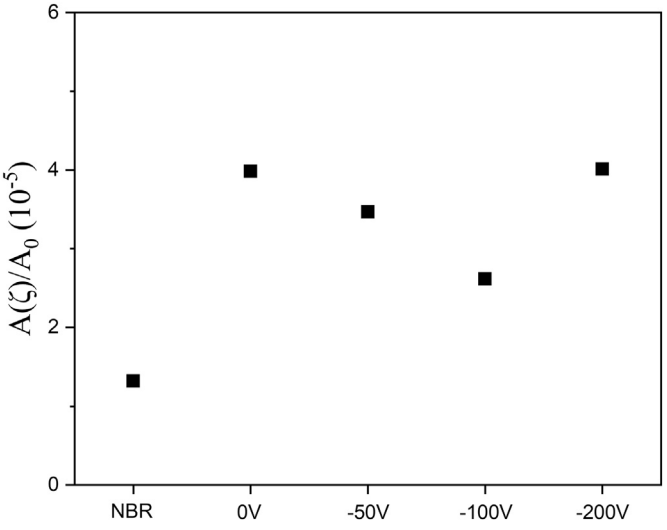

Fig. 15. The ratio of the actual contact area calculated to the nominal contact area, under the ζ = 5000, in the studied area of 5 × 5 μm^2, with the contact stress condition equivalent to the environment of mass of 460 g.

butadiene rubber (NBR) by the DC magnetron sputtering method were prepared under different substrate bias voltages. The tribo-performance and sealing property were discussed in detail. The DLC-coated NBR prepared with a bias voltage of −200 V exhibited excellent tribological performance as verified by the decreased coefficient of friction and a lower wear rate. This was attributed to the relatively enhanced hardness derived from a low sp^2/sp^3 ratio. In terms of sealing property, comparisons between experiments and theoretical calculations confirmed that the Young's modulus and the root-mean-square roughness yielded the low leakage rate of the DLC-coated NBR. Thus, the leakage rate could be regulated by the protective DLC films prepared under varied bias voltages.

Acknowledgements

This work was supported by Key Projects of Hainan Province (ZDYF2016019), Natural Science Foundation of China (51461015) and Natural Science Foundation of Hainan Province (518MS024).

References

[1] A. Tiwari, L. Dorogin, M. Tahir, K.W. Stöckelhuber, G. Heinrich, N. Espallargas, B.N.J. Persson, Rubber contact mechanics: adhesion, friction and leakage of seals, Soft Matter 13 (2017) 9103–9121, https://doi.org/10.1039/C7SM02038D.
[2] G. Capote, M.A. Ramírez, P.C.S. da Silva, D.C. Lugo, V.J. Trava-Airoldi, Improvement of the properties and the adherence of DLC coatings deposited using a modified pulsed-DC PECVD technique and an additional cathode, Surf. Coat. Technol. 308 (2016) 70–79, https://doi.org/10.1016/j.surfcoat.2016.08.096.
[3] W. Yue, C. Liu, Z. Fu, C. Wang, H. Huang, J. Liu, Synergistic effects between sulfurized W-DLC coating and MoDTC lubricating additive for improvement of tribological performance, Tribol. Int. 62 (2013) 117–123, https://doi.org/10.1016/j.triboint.2013.02.013.
[4] L. Chen, M.C. Yang, C.F. Song, B.J. Yu, L.M. Qian, Is 2nm DLC coating enough to resist the nanowear of silicon, Wear 302 (2013) 909–917, https://doi.org/10.1016/j.wear.2013.01.088.
[5] T. Nakahigashi, Y. Tanaka, K. Miyake, H. Oohara, Properties of flexible DLC film deposited by amplitude-modulated RF P-CVD, Tribol. Int. 37 (2004) 907–912, https://doi.org/10.1016/j.triboint.2004.07.007.
[6] M. Shen, F. Dong, Y. Ma, J. Peng, M.-H. Zhu, Fretting wear behaviors of acrylonitrile-butadiene rubber (NBR) against diamond-like carbon and graphene coatings, Int. J. Adv. Manuf. Technol. 96 (2017) 1749–1759, https://doi.org/10.1007/s00170-017-0946-1.
[7] S. Thirumalai, A. Hausberger, J.M. Lackner, W. Waldhauser, T. Schwarz, Anode layer source plasma-assisted hybrid deposition and characterization of diamond-like carbon coatings deposited on flexible substrates, Thin Solid Films 655 (2018) 54–61, https://doi.org/10.1016/j.tsf.2018.04.012.
[8] S. Thirumalai, A. Hausberger, J.M. Lackner, W. Waldhauser, T. Schwarz, Effect of the type of elastomeric substrate on the microstructural, surface and tribological characteristics of diamond-like carbon (DLC) coatings, Surf. Coat. Technol. 302 (2016) 244–254, https://doi.org/10.1016/j.surfcoat.2016.06.021.
[9] B.N.J. Persson, Contact mechanics for randomly rough surfaces, Surf. Sci. Rep. 61 (2006) 201–227, https://doi.org/10.1016/j.surfrep.2006.04.001.
[10] W. Dai, P. Ke, A. Wang, Influence of bias voltage on microstructure and properties of Al-containing diamond-like carbon films deposited by a hybrid ion beam system, Surf. Coat. Technol. 229 (2013) 217–221, https://doi.org/10.1016/j.surfcoat.2012.03.076.
[11] J.P. van der Pal, D. Martinez-Martinez, Y.T. Pei, P. Rudolf, J.T.M. De Hosson, Microstructure and tribological performance of diamond-like carbon films deposited on hydrogenated rubber, Thin Solid Films 524 (2012) 218–223, https://doi.org/10.1016/j.tsf.2012.10.005.
[12] National Center for Biotechnology Information, PubChem compd. Database, https://pubchem.ncbi.nlm.nih.gov/compound/702#section=Vapor-Pressure (n.d., accessed July 3, 2018).
[13] J. Hu, L. Wang, P. Zhang, C. Liang, G. Shao, Construction of solid-state Z-scheme carbon-modified TiO2/WO3 nanofibers with enhanced photocatalytic hydrogen production, J. Power Sources 328 (2016) 28–36, https://doi.org/10.1016/j.jpowsour.2016.08.001.
[14] A.C. Ferrari, J. Robertson, Interpretation of Raman spectra of disordered and amorphous carbon, Phys. Rev. B 61 (2000) 14095–14107, https://doi.org/10.1103/PhysRevB.61.14095.
[15] W. Xu, S. Lin, M. Dai, Q. Shi, C. Wei, X. Zhang, K. Zhou, Effects of bias voltage on the microstructure and properties of Al-doped hydrogenated amorphous carbon films synthesized by a hybrid deposition technique, Vacuum 154 (2018) 159–166, https://doi.org/10.1016/j.vacuum.2018.05.008.
[16] A.C. Ferrari, J. Robertson, Resonant Raman spectroscopy of disordered, amorphous, and diamondlike carbon, Phys. Rev. B 64 (2001) 75414, https://doi.org/10.1103/PhysRevB.64.075414.
[17] W.C. Oliver, G.M. Pharr, Measurement of hardness and elastic modulus by instrumented indentation: advances in understanding and refinements to methodology, J. Mater. Res. 19 (2004) 3–20, https://doi.org/10.1557/jmr.2004.19.1.3.
[18] C.-K. Liu, S. Lee, L.-P. Sung, T. Nguyen, Load-displacement relations for nanoindentation of viscoelastic materials, J. Appl. Phys. 100 (2006) 33503, https://doi.org/10.1063/1.2220649.
[19] B.J. Briscoe, K.S. Sebastian, M.J. Adams, The effect of indenter geometry on the elastic response to indentation, J. Phys. D. Appl. Phys. 27 (1994) 1156 http://stacks.iop.org/0022-3727/27/i=6/a=013.
[20] B.J. Briscoe, L. Fiori, E. Pelillo, Nano-indentation of polymeric surfaces, J. Phys. D. Appl. Phys. 31 (1998) 2395 http://stacks.iop.org/0022-3727/31/i=19/a=006.
[21] S. Yang, Y.-W. Zhang, K. Zeng, Analysis of nanoindentation creep for polymeric materials, J. Appl. Phys. 95 (2004) 3655–3666, https://doi.org/10.1063/1.1651341.
[22] Z. Qian, J. Risan, B. Stadnick, G.B. McKenna, Apparent depth-dependent modulus and hardness of polymers by nanoindentation: investigation of surface detection error and pressure effects, J. Polym. Sci. B Polym. Phys. 56 (2018) 414–428, https://doi.org/10.1002/polb.24554.
[23] F. Wen, N. Huang, H. Sun, J. Wang, Y.X. Leng, Synthesis of nitrogen incorporated carbon films by plasma immersion ion implantation and deposition, Surf. Coat. Technol. 186 (2004) 118–124, https://doi.org/10.1016/j.surfcoat.2004.04.040.
[24] D.E. Martínez-Tong, A.S. Najar, M. Soccio, A. Nogales, N. Bitinis, M.A. López-Manchado, T.A. Ezquerra, Quantitative mapping of mechanical properties in polylactic acid/natural rubber/organoclay bionanocomposites as revealed by nanoindentation with atomic force microscopy, Compos. Sci. Technol. 104 (2014) 34–39, https://doi.org/10.1016/j.compscitech.2014.08.030.
[25] P.H. Mott, J.R. Dorgan, C.M. Roland, The bulk modulus and Poisson's ratio of “incompressible” materials, J. Sound Vib. 312 (2008) 572–575, https://doi.org/10.1016/j.jsv.2008.01.026.
[26] Z. Xu, Y.J. Zheng, F. Jiang, Y.X. Leng, H. Sun, N. Huang, The microstructure and mechanical properties of multilayer diamond-like carbon films with different modulation ratios, Appl. Surf. Sci. 264 (2013) 207–212, https://doi.org/10.1016/j.apsusc.2012.10.003.
[27] N.G. Chechenin, J. Bøttiger, J.P. Krog, Nanoindentation of amorphous aluminum oxide films II. Critical parameters for the breakthrough and a membrane effect in thin hard films on soft substrates, Thin Solid Films 261 (1995) 228–235, https://doi.org/10.1016/S0040-6090(94)06494-6.
[28] S. Bhowmick, M.Z.U. Khan, A. Banerji, M.J. Lukitsch, A.T. Alpas, Low friction and wear behaviour of non-hydrogenated DLC (a-C) sliding against fluorinated tetrahedral amorphous carbon (ta-C-F) at elevated temperatures, Appl. Surf. Sci. 450 (2018) 274–283, https://doi.org/10.1016/j.apsusc.2018.04.023.
[29] A. Czyzniewski, Characterisation of transfer layer and wear debris on various counterparts sliding against undoped and doped DLC coatings, Plasma Process. Polym. 4 (2007) S231–S236, https://doi.org/10.1002/ppap.200730707.
[30] M. Lubwama, K.A. McDonnell, J.B. Kirabira, A. Sebbit, K. Sayers, D. Dowling, B. Corcoran, Characteristics and tribological performance of DLC and Si-DLC films deposited on nitrile rubber, Surf. Coat. Technol. 206 (2012) 4585–4593, https://doi.org/10.1016/j.surfcoat.2012.05.015.
[31] L. Cui, H. Zhou, K. Zhang, Z. Lu, X. Wang, Bias voltage dependence of superlubricity lifetime of hydrogenated amorphous carbon films in high vacuum, Tribol. Int. 117 (2018) 107–111, https://doi.org/10.1016/j.triboint.2017.08.020.
[32] M. Fujii, M. Ananth Kumar, A. Yoshida, Influence of DLC coating thickness on tribological characteristics under sliding rolling contact condition, Tribol. Int. 44 (2011) 1289–1295, https://doi.org/10.1016/j.triboint.2010.07.005.
[33] B.N.J. Persson, C. Yang, Theory of the leak-rate of seals, J. Phys. Condens. Matter 20 (2008) 315011, https://doi.org/10.1088/0953-8984/20/31/315011.
[34] G. Carbone, B. Lorenz, B.N.J. Persson, A. Wohlers, Contact mechanics and rubber friction for randomly rough surfaces with anisotropic statistical properties, Eur.

Phys. J. E 29 (2009) 275–284, https://doi.org/10.1140/epje/i2009-10484-8.
[35] B.N. Persson, O. Albohr, U. Tartaglino, A.I. Volokitin, E. Tosatti, On the nature of surface roughness with application to contact mechanics, sealing, rubber friction and adhesion, J. Phys. Condens. Matter 17 (2005) R1–R62, https://doi.org/10.1088/0953-8984/17/1/R01.
[36] A.P. Mousinho, R.D. Mansano, M.C. Salvadori, Influence of substrate surface topography in the deposition of nanostructured diamond-like carbon films by high density plasma chemical vapor deposition, Surf. Coat. Technol. 203 (2009) 1193–1198, https://doi.org/10.1016/j.surfcoat.2008.10.025.
[37] J.J. Quan, S.A. Wolf, H.N.G. Wadley, Low energy ion beam assisted deposition of a spin valve, J. Appl. Phys. 101 (2007) 074302, , https://doi.org/10.1063/1.2715751.
[38] H. Niakan, Q. Yang, J.A. Szpunar, Structure and properties of diamond-like carbon thin films synthesized by biased target ion beam deposition, Surf. Coat. Technol. 223 (2013) 11–16, https://doi.org/10.1016/j.surfcoat.2013.02.019.
[39] B. Elisabeth, Scaling properties of cracks, J. Phys. Condens. Matter 9 (1997) 4319 http://stacks.iop.org/0953-8984/9/i=21/a=002.